# Application of dual-focus fluorescence correlation spectroscopy to microfluidic flow-velocity measurement

**Tyler J. Arbour and Jörg Enderlein***

*Received 25th November 2009, Accepted 25th January 2010*
*First published as an Advance Article on the web 24th February 2010*
**DOI: 10.1039/b924594d**

Several methods exist to measure and map fluid velocities in microfluidic devices, which are vital to understanding properties on the micro- and nano-scale. Fluorescence correlation spectroscopy (FCS) is a method traditionally exploited for its ability to measure molecular diffusion coefficients. However, several reports during the past decade have shown that FCS can also be successfully used to measure precise flow rates in microfluidics with very high spatial resolution, making it a competitive alternative to other common flow-measurement methods. In 2007 we introduced a modified version of conventional FCS that overcomes many of the artifacts troubling the standard technique. Here we show how the advantages of this method, called dual-focus FCS, extend to flow measurements. To do so, we have measured the velocity flow profile along the cross-section of a square-bore microfluidic channel and compared the result to the theoretical prediction.

## Introduction

With the coming-of-age of microfluidic technology, many techniques have been developed to characterize behavior and properties of micro-scale systems. Effectively using a lab-on-a-chip approach in research and industrial applications requires comprehensive understanding of the system being used. As devices become smaller, the well-understood macroscopic behavior of a fluid can be affected significantly by the interaction of the sample with the walls of the microfluidic channel due to the increase in the surface area : volume ratio. Therefore, the measurement of fluid flow in microchannels, more specifically velocity and overall velocity profile of a flow, is one especially important area of interest. A closely related area of research is how surface properties of the channel material itself can affect flow behavior. Additionally, flow can be generated in more than one way, for *e.g.* with pressure or electroosmotically, and the resulting flow profiles will be very different in these two cases.[1] This is just one example that demonstrates the relevance of flow-profile mapping to our understanding of fluid behavior on the micro- and nano-scale.

Today, the microfluidics community has several tools with which to measure and map fluid flow. Among the most well-established are micro-particle image velocimetry (μPIV),[2,3] optical Doppler tomography,[4] UV photo-activation,[5] and fluorescence correlation spectroscopy (FCS).[6] A new method presented by Mushfique *et al.* uses optical tweezers to measure microfluidic flow velocity.[7] In comparison to the methods just mentioned, FCS stands out for several reasons.

One is spatial resolution, which is less than one micron laterally. Second is sensitivity—down to single molecules—which means that free fluorescent dyes at pico- to nanomolar concentration can be readily used as tracer particles, ensuring that the flow is not disrupted in any way. This is in contrast to other methods such as μPIV, which require particles with diameters measuring at least hundreds of nanometres (see ref. 2 and 3). A third attractive feature of FCS is its ability to accurately measure a wide dynamic range of flow velocities, as demonstrated by Brister *et al.* (2005), who used FCS to measure flow rates ranging over 4 orders of magnitude.[8] In this work, we will demonstrate how a modified version of FCS called dual-focus fluorescence correlation spectroscopy (2fFCS) introduces further significant advantages in the measurement of flow velocities by overcoming major limitations inherent to conventional FCS (1fFCS).

### History: fluorescence correlation spectroscopy and flow measurement

Fluorescence (sometimes helpfully called fluctuation) correlation spectroscopy relies on confocal optics to generate a very small detection volume—about a femtolitre—from which the fluorescence photons of single molecules in solution can easily be detected above the background signal. For freely diffusing molecules in solution, it is the fluctuations in the fluorescence signal over time (as molecules diffuse into and out of the detection volume) that reveal molecular hydrodynamic properties such as the diffusion coefficient. A natural extension of FCS is to the measurement of fluid flow, where the average time that molecules spend in the volume will be reduced, and the signal fluctuation will therefore change in a predictable manner.

The idea to extend FCS to flow measurements was first presented by its pioneers, Magde *et al.*, in a 1978 paper.[9] In that work, they not only spelled out the theory, but also validated the method experimentally by measuring fluid velocity using Rhodamine 6G in water. The next chapter in FCS flow measurement can be divided into two parts: (i) single-focus (1f) or conventional FCS and (ii) two-beam FCS, where the signals from two spatially separated confocal volumes are cross-correlated.[10,11] It is worth discussing the advantages of a cross-correlation in velocity measurements in a little more detail. We first

*III. Institute of Physics, Georg-August-Universität Göttingen, Friedrich-Hund-Platz 1, 37077 Göttingen, Germany. E-mail: joerg.enderlein@physik3.gwdg.de*

 

point out that in conventional FCS, the detection region is symmetric in the lateral dimensions, analogous to a perfect cylinder. As a consequence, the direction of the flow cannot be determined. In contrast, having two detection regions allows one to correlate the fluorescence fluctuations between them and thereby, under conditions of uniform flow, to determine the flow direction: A maximum in the cross-correlation will be observed at the time it takes a molecule to flow from the first to the second focus. Dittrich and Schwille nicely discussed single- *vs.* dual-beam modes of FCS in the context of transport within microfluidic structures, and went further by comparing and contrasting one- and two-photon excitation for both cases.[12]

In 2001, Gösch *et al.* showed how conventional FCS could be used for hydrodynamic flow profiling, *i.e.* to map the entire (laminar) flow field by scanning the confocal spot incrementally through a 50 × 50 μm channel (ref. 6). More recently, similar work was done in the Weston group, where the aim was to use single-focus FCS as a tool for flow-velocity imaging.[8,13] Ref. 8 contains an excellent and comprehensive discussion of 1fFCS applied to flow rate measurements, including optimization, limitations and artifacts, borrowing from the authors' title.

### Dual-focus fluorescence correlation spectroscopy

Dual-focus (2f) FCS, which was recently developed in our group, overcomes some major limitations and artifacts of the conventional technique.[14] As mentioned above, the concept of using more than one focus and cross-correlation in FCS has been demonstrated before. However, 2fFCS relies on subtle but key differences in the way the two foci are generated, their spatial separation, and in the way excitation and detection are performed. Before describing the method in more detail, a discussion of the main experimental artifacts that arise in conventional FCS measurements is needed.

As introduced above, FCS is based on the detected signal fluctuations in time as fluorescent species in solution travel—either by purely random diffusion or diffusion plus directed flow—through an open volume element. In order to accurately relate the mean time of a single-molecule transit to hydrodynamic properties, knowledge of the size and shape of the detection volume (or molecule detection function) is crucial. Although it may be trivial to calculate the volume's size and shape based on theory, there are many hard-to-control experimental parameters that can distort this ideal theoretical shape.[15,16] The most important of these are microscope slide thickness deviation, sample refractive index mismatch (and thus temperature), laser beam geometry, and perhaps most disturbing, excitation intensity (due to optical saturation), see *e.g.* ref. 17. The cumulative and often unknown result of these effects requires that frequent, time-consuming calibration be performed when using conventional FCS. These artifacts limit the usefulness of 1fFCS as a quantitative method.

2fFCS is able to overcome the dependence on these troubling experimental details in a simple way: introducing a constant, known distance into the confocal geometry scheme, namely the distance between the two focal axes. The distance can be determined very precisely, for example 370 ± 1.5 nm (RSD = 0.4%) for $\lambda_{ex} = 470$ nm.[18] The length of this so-called external ruler is a function of only two parameters: (i) excitation wavelength and (ii) the optical properties of the Nomarski prism used to spatially shift a single laser beam into two foci based on (orthogonal) polarization. The details of the setup have been described previously in ref. 14, and we explain in the Methods section below how the length of this external ruler is determined and periodically checked for a 2fFCS setup.

In contrast to other two-beam methods, 2fFCS makes use of the intentional overlap of the two detection regions. Normally, spatial overlap is detrimental because it leads to a "pseudo-autocorrelation" that distorts the measurements (ref. 11). We overcome this issue by using pulsed interleaved excitation (PIE)[19,20] in which the two excitation sources (corresponding to the two confocal detection volumes) pulse in an alternating fashion. This makes it possible to distinguish between focus 1 and focus 2 as the source of the detected photon. A comparison of optical saturation effects in 1f- and 2fFCS is the subject of ref. 21.

One of the most impressive set of results using 2fFCS, and one that illustrates how it represents a significant advance from existing techniques, come from a meticulous study by Müller *et al.* in 2008 (ref. 18). Müller and colleagues used the new method to measure the diffusion coefficients of widely used reference dyes with peak absorption across the visible spectrum. The results were striking. For example, they measured a diffusion coefficient for Rhodamine 6G that is 37% larger than the reference value used in most FCS publications over the last three decades. Again, the reason for the discrepancies is that conventional FCS has huge problems in precisely determining the spatial extension of the molecule detection function, which depends not only on the optical setup, but also on the photophysical properties of the used dyes in conjunction with the used laser excitation intensity during a measurement. The same systematic errors seen in measuring diffusion coefficients with FCS translate into analogous systematic errors when measuring flow velocities. The same advantages that 2fFCS brings to diffusion coefficient measurements also apply to velocity measurements, because in both cases one has an extrinsic and unchanging length scale, the distance between foci.

In short, 2fFCS is able to yield absolute values of hydrodynamic properties without calibration. Showing how these and other advantages apply to flow-velocity measurement is the aim of this paper.

## Theory

Hydrodynamic properties are revealed by the shape and temporal decay of the auto- and cross-correlation functions of a 2fFCS measurement. The quantitative heart of the method, therefore, is the calculation and subsequent fit of this function. Although 2fFCS introduces an external length scale into the experiment, determined by the distance $d$ between the two foci, one still needs a generic model for the shape of each detection volume. This shape is quantitatively defined by the so-called molecule detection function (MDF), which describes the efficiency of exciting and detecting a photon from a single molecule at a given position $r$ within the sample. As was shown in ref. 14 and 22, a sufficiently good approximation of the (non-shifted, axially centered) MDF is given by a modified Lorentz–Gauss curve of the form:

$$U(r) = \frac{\kappa(z)}{w^2(z)} \exp\left[ -\frac{2(x^2+y^2)}{w^2(z)} \right] \quad (1)$$

where the $x$, $y$ and $z$ are Cartesian coordinates with the $z$-axis along the optical axis. The functions $\kappa(z)$ and $w(z)$ are defined by:

$$w(z) = w_0 \left[ 1 + \left( \frac{\lambda_{ex} z}{\pi w_0^2 n} \right)^2 \right]^{1/2} \quad (2)$$

and

$$R(z) = R_0 \left[ 1 + \left( \frac{\lambda_{em} z}{\pi R_0^2 n} \right)^2 \right]^{1/2} \quad (3)$$

where $\lambda_{ex}$ is the excitation wavelength, $\lambda_{em}$ the center emission wavelength, $n$ is the refractive index of the immersion medium (water), $a$ is the radius of the confocal aperture divided by magnification, and $w_0$ and $R_0$ are two model parameters (for more details and validation of this model, see ref. 14 and 22).

With knowledge of the MDF, the calculation of the auto- and cross-correlation functions of a 2fFCS measurement with diffusing and flowing sample is straightforward. The probability to find a molecule within the infinitesimally small volume $dr_0$ at any position $r_0$ is given by the product of concentration $c$ and volume $dr_0$. The chance to detect a photon from such a molecule at position $r_0$ is described by the MDF itself. The probability that this molecule moves, within time $t$, from its initial position $r_0$ to a new position $r_1$, is given by the solution to the diffusion–convection equation:

$$\frac{\partial G(r_1 - r_0, t)}{\partial t} + v \times \bar{\nabla} G(r_1 - r_0, t) = D \Delta G(r_1 - r_0, t) \quad (4)$$

with initial condition

$$\lim_{t \to 0} G(r_1 - r_0, t) = \delta(r_1 - r_0) \quad (5)$$

where $D$ is the diffusion coefficient, the velocity field $v$ is assumed to be constant and homogenous over the detection region, and $\delta(r_1 - r_0)$ denotes Dirac's delta-function. The solution to this equation is then given by:

$$G(r_1 - r_0, t) = \frac{1}{(4\pi D t)^{3/2}} \exp\left[ -\frac{|r_1 - r_0 - vt|^2}{4Dt} \right] \quad (6)$$

Finally, the chance to detect a second photon from the molecule at its new position is again given by the corresponding MDF. Putting everything together yields the following expression for the correlation function:

$$g_{jk}(t) = g_\infty + \varepsilon_j \varepsilon_k c \int dr_0 \int dr_1 U_k(r_1) G(r_1 - r_0, t) U_j(r_0) \quad (7)$$

where $g_\infty$ is some constant offset at $t \to \infty$, and the $\varepsilon_j$, $j = 1, 2$, account for the global excitation and detection efficiency of the measurement setup. The indices $j$ and $k$ refer to the two possible MDFs in a 2fFCS experiment, which are given by eqn (1), only laterally shifted by a value $d/2$ to each side of the optical axis (*e.g.* along the $x$-axis). If $j = k = 1$, one obtains the autocorrelation function for the first focus, if $j = k = 2$ that for the second, if $j = 1$ and $k = 2$, one has the cross-correlation function from the first to the second focus, and correspondingly $j = 2$ and $k = 1$ yield the cross-correlation from the second to the first focus. By shifting the variables of integration by an amount of $\pm(d/2) \times e_x$ and performing the integrations over $x$ and $y$, the expression for the correlation functions simplifies to:

$$g(t, \delta) = g_\infty + \varepsilon_j \varepsilon_k \frac{c}{4} \sqrt{\frac{\pi}{Dt}} \int dz_1 \int dz_2 \frac{\kappa(z_1)\kappa(z_2)}{8Dt + w^2(z_1) + w^2(z_2)} \times \exp\left[ -\frac{(z_2 - z_1 - v_z t)^2}{4Dt} - 2\frac{(\delta - v_x t)^2 + v_y^2 t^2}{8Dt + w^2(z_1) + w^2(z_2)} \right] \quad (8)$$

where one has to set $\delta = 0$ and $j = k = 1$ or $j = k = 2$ for the two autocorrelation functions, respectively; $\delta = +d$, $j = 1$, and $k = 2$ for the cross-correlation from first to second focus, and $\delta = -d$, $j = 2$, and $k = 1$ for the cross-correlation from second to first focus.

The expression of eqn (8) cannot be simplified further and must be evaluated numerically when fitting experimental curves. In doing so, it is convenient to change variables to:

$$\xi = \frac{z_2 - z_1}{2\sqrt{Dt}}, \quad \eta = \frac{z_2 + z_1}{2} \quad (9)$$

leading to the expression

$$g(t, \delta, v) = g_\infty + \frac{\varepsilon_j \varepsilon_k c \sqrt{\pi}}{2} \int d\xi \int d\eta \frac{\kappa(\zeta_-)\kappa(\zeta_+)}{8Dt + w^2(\zeta_-) + w^2(\zeta_+)} \times \exp\left[ -\left( \xi - \frac{v_z}{2}\sqrt{\frac{t}{D}} \right)^2 - \frac{2(\delta - v_x t)^2 + 2(v_y t)^2}{8Dt + w^2(\zeta_-) + w^2(\zeta_+)} \right] \quad (10)$$

where $\zeta_\pm = \eta \pm (Dt)^{1/2}\xi$. Because $w$ and $\kappa$ are rapidly decaying functions for large argument, the infinite integrations over $\eta$ and $\xi$ can be approximated by numerically evaluating the integrals within a finite two-dimensional strip defined by $|\zeta_\pm| < M$, where $M$ is a truncation value chosen in such a way that the numerical integration result does not change when increasing $M$ further. Numerical integration is done by using a simple finite element scheme. Convergence is checked by testing whether the numerical result does not change upon refining the finite element size and when increasing the threshold value $M$.

Data fitting is performed with least-square fitting of the model curve, eqn (10), against the four measured correlation functions in a global fit. As fit parameters one has $\varepsilon_1 c^{1/2}$, $\varepsilon_2 c^{1/2}$, $D$, $w_0$ and $R_0$, as well as three offset values $g_\infty$. The distance $d$ between the detection regions is determined by the properties of the Nomarski prism and is known *a priori*. It is important to notice that a crucial criterion of fit quality is not only to simultaneously reproduce the temporal shape of all correlation functions, but also to reproduce their relative amplitude ratio.

## Materials and methods

A simple microfluidic model system was constructed: laminar flow of the sample solution was generated using a syringe pump (Nexus 3000, Chemyx) and 1 mL Luer Lock® syringe (SGE). The solution was pumped, *via* PVC tubing (Cole-Parmer, 0.065″ id, length 24″), through a 300 × 300 μm² (inner dimensions) square bore capillary (Vitrocom, Mountain Lakes, NJ, USA), which was mounted on a custom-made holder designed for use

with an inverted microscope. The sample solution used for all experiments was aqueous Oregon Green 488 (Invitrogen) fluorescent dye at nanomolar concentration, made by diluting the stock dye solution with triple-distilled water.

2fFCS measurements were performed using an inverse time-resolved fluorescence microscope (MicroTime 200, PicoQuant GmbH, Berlin, Germany) equipped with a 60×, 1.2 N.A. water immersion objective. The 2fFCS setup has been described previously (ref. 14 and 23), and the key concepts are reviewed in the following subsection. Pulsed interleaved excitation (PIE, ref. 19) was accomplished using the system's two 470 nm diode lasers. In this method, the lasers were pulsed alternately, each with 50 ns delay. Excitation and emission photons passed through the same objective. A tube lens focused the light onto a single pinhole (slightly larger than in 1fFCS to accommodate both foci), and the fluorescence emission was then split with a 50/50 beam splitter onto two identical SPAD detectors to overcome afterpulsing effects (see *e.g.* ref. 24).

For each flow-profile acquisition, the confocal spot was manually scanned in the direction of the optical axis ($z$-direction) using the microscope's vertical adjustment knob (scale in micrometres). The position of the inner capillary surface nearest the objective (designated as the zero position) was found by observing the Airy discs (using the MicroTime 200's CCD camera) at the outer and then inner glass surfaces. Measurement at each position was continued until at least 7 million photon-detection events had been recorded (as determined directly from file size), typically requiring 5 to 10 minutes. The input volumetric flow rate was 38 μL $min^{-1}$ for the flow-profile scans, corresponding to a bulk linear fluid velocity of ~7 mm $s^{-1}$. Laser excitation intensity was 50 μW for the flow-profile scans and 10 μW for the no-flow reference measurements.

Data analysis and fitting were performed using custom Matlab routines. The general fitting approach was as follows. For each flow-profile acquisition, a reference measurement was made at zero-flow conditions (free diffusion of the fluorophores) at the optimal height of 30 μm above the capillary surface. The values of $w_0$ and $R_0$ resulting from a best fit of this measurement data (see Theory for a description of the free parameters) were fixed for subsequent flow-velocity data fitting. Error estimation was achieved by partitioning the data of individual measurements into bins of $10^6$ photon-detection events. Each bin was then fitted separately to find the measured velocity, allowing an estimated standard deviation to be calculated.

### Dual-focus FCS setup and initial calibration

The most important requirements for 2fFCS are a laser beam composed of two orthogonal plane-polarized radiation vectors, and a Nomarski or "DIC" prism, normally used for differential interference contrast microscopy. While the simplest way to create such a laser beam is to use two linearly polarized pulsed diode lasers, another scheme has been shown to work that utilizes only one.[25] Our setup includes two lasers, whose light is combined by a polarizing beam splitter and then sent through one polarization-preserving, single-mode fiber. The single-laser setup presented in ref. 25 accomplishes the same feat with an electro-optical modulator, which can easily be added to 1fFCS instrument.

The critical parameter that must be determined for a 2fFCS setup is the distance between the two foci. Ref. 18 includes the most precise determination of the interfocal distance, achieved by performing a comparative measurement of fluorescent beads using dynamic light scattering (DLS) and 2fFCS. Alternatively, thanks to the groundwork laid in that study, one can use the reference values of dye diffusion as given in the cited paper for calibrating new 2fFCS setups. A typical distance and precision that can be expected is 370 ± 1.5 nm (RSD = 0.4%) for $\lambda_{ex}$ = 470 nm.

## Results and discussion

The microcapillary was aligned in one of two orthogonal orientations, relative to the dual-focus confocal geometry, for all flow measurements. To help make this clearer, and introduce the

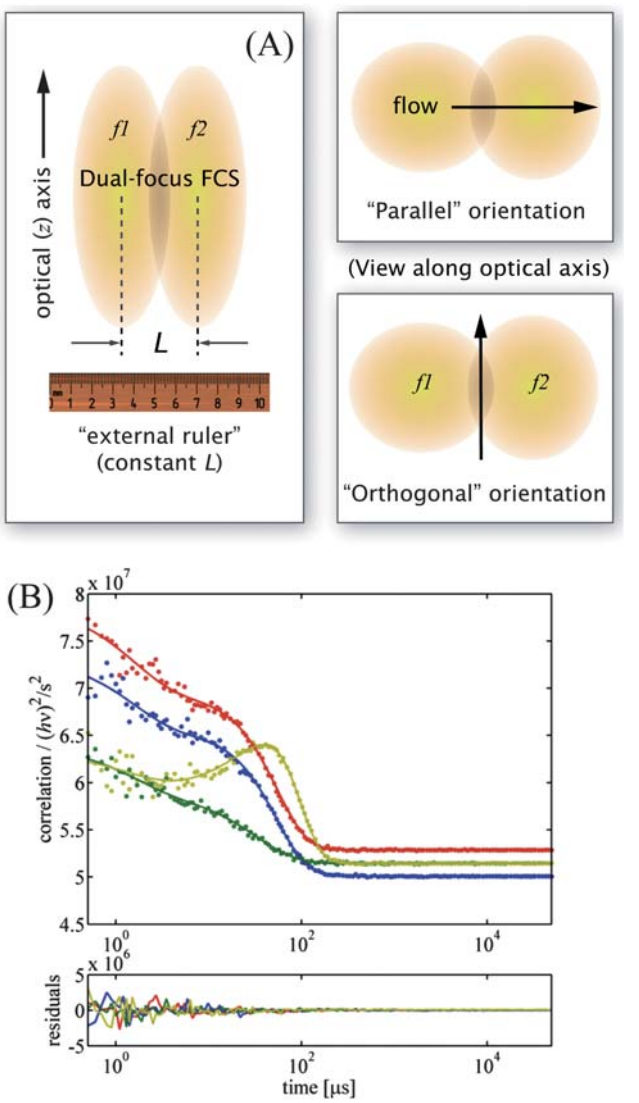


**Fig. 1** (A) Graphic visualization of the 2fFCS confocal volume and the nomenclature we use to describe its orientation relative to the direction of flow. (B) Typical fitted 2fFCS correlation curves. The four curves are comprised of two autocorrelations (one from each focus) and the forward and reverse cross-correlations. The data shown are for flow measurement in the "parallel" orientation, and therefore show a maximum in the "forward" cross-correlation.

nomenclature that will henceforth be used to indicate orientation, Fig. 1A includes a visual representation. The left picture is meant to represent the overlapping confocal volumes, which have arbitrarily been labeled f1 and f2; the "external ruler" stresses the importance of the fixed distance between the focal axes. The right-hand figure boxes explain our convention of referring to the interfocal flow vector (f1 to f2) as "parallel" and the perpendicular flow vector as "orthogonal." The motivation to use these two "extreme" orientations (90° relative rotation) was that if the velocity could be accurately measured in either orientation, then it follows that the 2D-velocity vector can be well-resolved given any flow direction (or, equivalently, any orientation of the foci).

With this geometric picture in mind, one can get a sense of the spatial resolution of FCS. The MDF is elongated in the direction of the optical axis, therefore the best resolution can be achieved by scanning in the lateral plane, orthonormal to this. Roughly, resolutions in the $z$ and lateral ($x$, $y$) directions are about 1 and 0.5 microns, respectively. Unfortunately for FCS, this means that resolution near the capillary wall is at its worst, since the surface must be normal to the optical axis. Measurement in the near-wall region is discussed in more detail below.

To introduce readers to what the processed data look like, typical fitted 2fFCS correlation curves for the parallel orientation are shown in Fig. 1B. The four curves are derived from an autocorrelation from each focus (red, blue) and the forward and reverse cross-correlations (yellow and green, respectively). The characteristic maximum observed in the forward cross-correlation occurs at the time that it takes a fluorophore to flow from f1 to f2. Conveniently, this feature allows one to accurately estimate the velocity, even without fitting the autocorrelation curves, because the distance between the two foci is well-known and fixed. Note that this peak is only observed in the "forward" cross-correlation and not in the "reverse," indicating the ability of 2fFCS to resolve the direction of flow. Additionally, it is noted that the rich structure of the 2fFCS correlations makes the fitting procedure much less ambiguous than for 1fFCS.

The Hagen–Poiseuille equation predicts that laminar flow in a pipe of circular cross-section will follow a parabolic velocity profile. The slightly modified theoretical prediction for the case of a rectangular duct[26] and corresponding experimental results are plotted in Fig. 2A and B. The measured flow-velocity profile for each of the two orientations agrees remarkably well with the theoretical prediction. Perhaps surprisingly, the relative standard

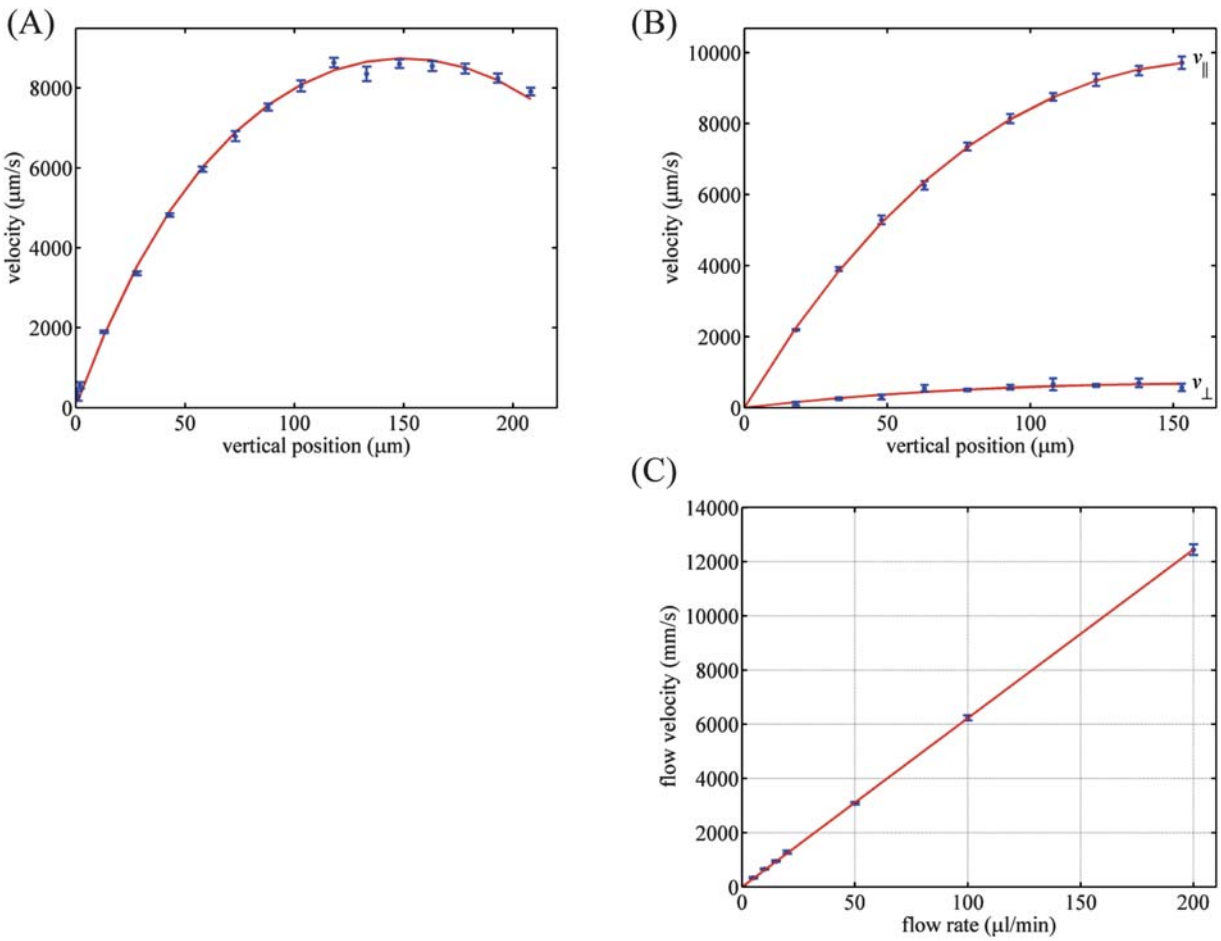


**Fig. 2** Measured flow-velocity profiles in the (A) parallel orientation (flow parallel to interfocal axis) and (B) orthogonal orientation. When fitting the orthogonal-flow data the parallel-velocity parameter was not fixed to zero, and the resulting profile ($v_{\parallel}$) indicates a 4-degree misalignment of the microcapillary. (C) Measured flow speed is plotted against the volumetric flow rate input to the syringe pump. The high degree of linearity and small error bars demonstrate 2fFCS's flow measurement precision over a wide dynamic range of flow rates. Table 1 shows RSD values for (A) and (B).

**Table 1** The relative standard deviations for each data point in the large-amplitude curves of Fig. 2A and B

| Vertical position/μm | % RSD (A) | % RSD (B) |
|---|---|---|
| 15 | 0.9 | 1.7 |
| 30 | 1.3 | 1.4 |
| 45 | 2.4 | 0.9 |
| 60 | 1.8 | 1.1 |
| 75 | 1.5 | 1.8 |
| 90 | 1.5 | 1.1 |
| 105 | 1.3 | 1.7 |
| 120 | 1.9 | 1.4 |
| 135 | 1.4 | 2.2 |
| 150 | 1.8 | 1.2 |

deviation (as determined by identical successive measurements) of the flow velocity for the orthogonal orientation was just as good as that of the parallel arrangement as shown in Table 1. This supports the claim that 2fFCS can resolve the *x*- and *y*-components of flow velocity simultaneously—a feature that neither 1f- nor other two-beam FCS methods can claim. Further fortuitous support is found in Fig. 2B: the accidental misalignment of the capillary relative to the interfocal axis led to an apparent non-zero parallel velocity component. This velocity component was left as a free parameter during fitting and we see that, indeed, we can resolve both the *x*- and *y*-velocity vectors. A simple calculation shows that the misalignment of the capillary was 4°.

In FCS, an analytic statistical analysis of the error in a measured parameter of interest, such as the diffusion coefficient or the velocity, is not possible. This is due to the highly nonlinear connection between the events one is observing, *i.e.* fluorescence fluctuations due to molecules passing through the detection volume, and the final velocity value, the latter being obtained through a fit of the so-called autocorrelation function. Ref. 27 provides a theoretical treatment of the statistics of FCS-measured values. Many years of experience in FCS have convinced us that the most reliable and telling account of error is simply through subsequent repetition of measurements. This procedure was used in these experiments to generate the error bars shown (see Methods).

Conventional FCS has previously been used to map velocity profiles, most recently by the Weston group (ref. 8 and 13). Therefore, a discussion of the specific advantages of 2fFCS over 1fFCS in the context of flow measurement is in order (in addition to the unique ability of 2fFCS to measure flow direction over 360°). As discussed in the introduction, the major setbacks of FCS derive from distortion of the molecule detection function (MDF). The most influential parameter is the laser beam waist radius, conventionally called $w_0$. Rigorous theoretical treatments of 2fFCS and 1fFCS can be found in ref. 22, 23 and 28. As with all FCS measurements (and as noted by Brister *et al.*, ref. 8), the accuracy of the velocities determined by 1fFCS depends on the accuracy in the value of $w_0$ for the instrument, and is normally the largest source of systematic error. Extremely slight variation in experimental parameters such as temperature, cover-slide thickness, refractive index, and excitation intensity will cause distortion of the very touchy MDF. Dual-focus FCS largely overcomes this problem through the introduction of an external ruler, *i.e.* the known and fixed distance between the two focal volumes (Fig. 1A). The ruler becomes the major geometric parameter of the system, instead of MDF parameters like $w_0$. What this means for experimental application is greatly increased accuracy and reliability without calibration. Quantitative FCS flow measurements can now be achieved simply and quickly.

Distortion of the confocal volume becomes even more pronounced near the capillary wall. Since distortion is much less of an issue for 2fFCS, the method is much more adept at probing the near-wall region than 1fFCS. As already stated, the spatial resolution in this region of large velocity gradient is only ~1 μm, meaning that other techniques such as total internal reflection velocimetry (TIRV)[29] are more suited for probing the near-wall (less than 300 nm) region, although the possibility of artifactual surface effects on the relatively large tracer particles is worrisome. Still, we expect that it should be possible to make accurate measurements as close as 1.0 microns from the surface, corresponding to a point at which a substantial portion of the confocal "egg" is being cut off. The first data point in Fig. 2A was taken at 2–3 μm from the surface, and we have obtained good results slightly closer than this (data not shown). The RSD will, of course, be higher in this region due to much lower flow rates. For example the two leftmost points in Fig. 2A have RSD of 42% and 14%, respectively.

Although temporal resolution was not the subject of this study, its importance necessitates a brief discussion. Temporal resolution is not a strongpoint of FCS, and this is equally true for 1f- and 2fFCS. Minimizing the time required to map the flow field was the major goal in the study by Brister *et al.* (ref. 8), and because their results apply to FCS in general, we did not attempt to repeat their analysis.

Temporal resolution can be increased in the following ways, each having certain tradeoffs: (i) brighter particles (*e.g.* fluorescent beads); Brister *et al.* used 40 nm beads, which drastically reduce the measurement time needed because of the increased photon flux. Clearly, the effects of the particles themselves on the flow field become an issue as tracer size increases. Also, optical saturation capable of damaging the detector becomes a problem, especially at higher tracer concentrations. The authors noted that they had to reduce the laser intensity at higher concentrations to avoid such damage and the measurement artifacts incurred. (ii) Increased laser excitation power. Here, 2fFCS has a huge advantage over conventional, as the measurement-skewing effects of optical saturation are dramatically reduced (see ref. 21). Brister *et al.* found, using optimized conditions with the 40 nm beads, that velocity measurements with precision of 5% RSD could be achieved in less than 200 milliseconds (single point, not the entire scan). At this rate, a single 2D slice of the flow profile for a 100 μm id capillary using 1 μm steps could be obtained in *ca.* 20 seconds.

An outstanding feature of FCS applied to flow measurement is the wide dynamic range over which it is able to measure. Brister *et al.* found that they were able to measure accurately over *ca.* 4 orders of magnitude, showing experimentally that the velocity *vs.* pressure relation is highly linear over a range from about 10 to more than 1200 mm $s^{-1}$. We performed a similarly linearity check at the low end of this scale, shown in Fig. 2C. The measured velocities, when plotted against the volumetric flow rate input to the syringe pump, display highly linear behavior down to the

lowest velocities measured (*ca.* 200 μm $s^{-1}$). It is also expected that 2fFCS will yield more accurate results at higher flow velocities due to the larger overall size of the dual-focus geometry, although we did not explore this experimentally. The important point is that 2fFCS extends the already impressive range for FCS-velocity measurements, especially the low-velocity limit.

## Conclusions

Research conducted in this group and those of our collaborators during the past few years has shown that dual-focus FCS measurements are more robust than the conventional method against experimental artifacts. The dual-focus modification, and resulting external length scale hallmark, makes FCS much more useful and reliable as a quantitative method, yielding molecular hydrodynamic properties such as the diffusion coefficient without calibration. This freedom from calibration and increased accuracy extend to flow-velocity measurements, making 2fFCS one of the simplest and most reliable techniques available for accurate measurement of flow velocities and profiles.

## Acknowledgements

T.J.A. would like to thank the German Academic Exchange Service (DAAD) for helping to make this research possible and for an enriching, unforgettable year in Germany. Financial support from the Deutsche Volkswagenstiftung is also gratefully acknowledged. Finally, T.J.A. must thank excellent colleagues, especially Anastasia Loman, Jana Humpolíčková, Ingo Gregor and Bernd Müller for abundant help and enlightening discussions.

## References

1 T. M. Squires and S. R. Quake, *Rev. Mod. Phys.*, 2005, **77**, 977–1026.
2 J. G. Santiago, S. T. Wereley, C. D. Meinhart, D. J. Beebe and R. J. Adrian, *Exp. Fluids*, 1998, **25**, 316–319.
3 C. D. Meinhart, S. T. Wereley and J. G. Santiago, *Exp. Fluids*, 1999, **27**, 414–419.
4 X. J. Wang, T. E. Milner and J. S. Nelson, *Opt. Lett.*, 1995, **20**, 1337–1339.
5 W. R. Lempert, K. Magee, P. Ronney, K. R. Gee and R. P. Haugland, *Exp. Fluids*, 1995, **18**, 249–257.
6 M. Gösch, H. Blom, J. Holm, T. Heino and R. Rigler, *Anal. Chem.*, 2000, **72**, 3260–3265.
7 H. Mushfique, J. Leach, H. B. Yin, R. Di Leonardo, M. J. Padgett and J. M. Cooper, *Anal. Chem.*, 2008, **80**, 4237–4240.
8 P. C. Brister, K. K. Kuricheti, V. Buschmann and K. D. Weston, *Lab Chip*, 2005, **5**, 785–791.
9 D. Magde, W. W. Webb and E. L. Elson, *Biopolymers*, 1978, **17**, 361–376.
10 M. Brinkmeier, K. Dorre, K. Riebeseel and R. Rigler, *Biophys. Chem.*, 1997, **66**, 229–239.
11 M. Brinkmeier, K. Dorre, J. Stephan and M. Eigen, *Anal. Chem.*, 1999, **71**, 609–616.
12 P. S. Dittrich and P. Schwille, *Anal. Chem.*, 2002, **74**, 4472–4479.
13 K. K. Kuricheti, V. Buschmann and K. D. Weston, *Appl. Spectrosc.*, 2004, **58**, 1180–1186.
14 T. Dertinger, V. Pacheco, I. von der Hocht, R. Hartmann, I. Gregor and J. Enderlein, *ChemPhysChem*, 2007, **8**, 433–443.
15 J. Enderlein, I. Gregor, D. Patra and J. Fitter, *Curr. Pharm. Biotechnol.*, 2004, **5**, 155–161.
16 J. Enderlein, I. Gregor, D. Patra, T. Dertinger and B. Kaupp, *ChemPhysChem*, 2005, **6**, 2324–2336.
17 I. Gregor, D. Patra and J. Enderlein, *ChemPhysChem*, 2005, **6**, 164–170.
18 C. B. Müller, A. Loman, V. Pacheco, F. Koberling, D. Willbold, W. Richtering and J. Enderlein, *Europhys. Lett.*, 2008, **83**, 46001.
19 B. K. Müller, E. Zaychikov, C. Bräuchle and D. C. Lamb, *Biophys. J.*, 2005, **89**, 3508–3522.
20 A. N. Kapanidis, T. A. Laurence, N. K. Lee, E. Margeat, X. X. Kong and S. Weiss, *Acc. Chem. Res.*, 2005, **38**, 523–533.
21 A. Loman, T. Dertinger, F. Koberling and J. Enderlein, *Chem. Phys. Lett.*, 2008, **459**, 18–21.
22 J. Enderlein, I. Gregor, D. Patra, T. Dertinger and U. B. Kaupp, *ChemPhysChem*, 2005, **6**, 2324–2336.
23 T. Dertinger, A. Loman, B. Ewers, C. B. Müller, B. Kramer and J. Enderlein, *Opt. Express*, 2008, **16**, 14353–14368.
24 J. Enderlein and I. Gregor, *Rev. Sci. Instrum.*, 2005, **76**, 033102.
25 Y. Korlann, T. Dertinger, X. Michalet, S. Weiss and J. Enderlein, *Opt. Express*, 2008, **16**, 14609–14616.
26 D. B. Holmes and J. R. Vermeule, *Chem. Eng. Sci.*, 1968, **23**, 717–722.
27 J. Enderlein, I. Gregor, D. Patra and J. Fitter, *J. Fluoresc.*, 2005, **15**, 415–422.
28 J. Enderlein, I. Gregor, D. Patra and J. Fitter, *Curr. Pharm. Biotechnol.*, 2004, **5**, 155–161.
29 P. Huang and K. S. Breuer, *Phys. Fluids*, 2007, **19**, 028104.

 